A Bidirectional Multi-Port Structure of DC-DC Converter for Energy Storage Systems

Hossein Shayeghi[1,*], **Saeed Pourjafar**[2], **and J. A. López-Villanueva**[3]

[1,2] *Energy Management Research Center, University of Mohaghegh Ardabili, Ardabil, Iran*
[3] *Department of Electronics and Computer Science, University of Granada, Spain*
[*] *Corresponding author email: hshayeghi@gmail.com*

Manuscript received 25 July, 2022; revised 11 November , 2022; accepted 27 November, 2022. Paper no. JEMT-2207-1402.

This study proposes a multi-port bidirectional DC-DC topology for energy storage usages. This topology can share a bidirectional power flow between the input and output ports. Also, by adjusting the duty cycles of the power switches, it can operate in boost and buck mode. The suggested topology has three ports, a low voltage side, a high voltage side, and one auxiliary port. In the structure of the proposed converter only three power switches and two inductors are used. Therefore, other advantages of this converter are low component count and high efficiency. To illustrate the performance and effectiveness of the recommended topology, technical statues and steady-state survey, design procedure, efficiency calculation, and comparison assessment are provided. Finally, to verify the theoretical investigation, an experimental prototype with capability to operate in boost and buck operation, with 170 W rated power in boost mode and 90 W in buck mode, with 50 kHz switching frequency is built and its results are presented.

keywords: *Bidirectional DC-DC Converter, High voltage gain, Low voltage stress, Low component count*

http://dx.doi.org/10.22109/JEMT.2022.353389.1402

1. INTRODUCTION

In recent years, due to the economic and environmental issues, electric vehicles (EVs) and hybrid electric vehicles (HEVs) applications have increased [1, 2]. On the other hand, overuse of the fossil fuel increases the greenhouse gases generation. Therefore, researchers have tried to find and resolve the problems of green energies such as photovoltaic (PV) and wind. Hybrid energy systems (HESs) have been utilized in EVs with the aim of battery charging component usage with an acceptable reliability [3, 4]. In HESs, bidirectional power flow should be provided to charge and discharge ESs. The other required features of these systems are low number of used components, low cost and volume, and high efficiency [5, 6].

DC-DC power topologies can be separated into two main categories: bidirectional and unidirectional topologies. The unidirectional converters such as classical boost converter only deliver power from input port to output port with increased voltage [7, 8]. But in many applications like HES and renewable energy, bidirectional power flow is necessary to have an ideal and reliable system. Additionally, in such applications, there are two or more power sources. Thus, a single-input single-output power converter couldn't be helpful. To resolve this significant problem of DC-DC converters, researchers proposed multi-port structures [9, 10]. Fig. 1 depicts the application of the multi-port bidirectional DC-DC structure for EV with HESs. As shown in this figure, a PV array along with a storage element like battery can deliver power to the output port with a bidirectional power flow. The other feature that should be provided in a multi-port converter is simultaneously and/or individually transferring power from input to output sources [11, 12]. It means that, when one input supply is switched off, the other one can provide the needed energy [12]. Recently, many types of multi-port DC-DC topologies via bidirectional or unidirectional feature have been proposed.

In [13–15], three input single-output converters with bidirectional feature was reported for hybrid PV, fuel cell (FC), and battery usages. These topologies are obtained using combination of a classical buck-boost and a boost structure with higher voltage gain than conventional step-up topology. They use one unidirectional port and one bidirectional port, which makes them suitable for hybrid generation usages. A transformer-less bidirectional multi-port topology was presented in [16] for EVs with HESs. By controlling the active power sharing, this topology can adjust the power of ESs. Also, it has boost and buck operation and the input voltages can be greater or smaller than the output voltage. However, one diode, one switch and one inductor are needed to extend the input ports, which improve the cost and mass of the converter. In [17], using the conventional buck-boost converter a two-input high gain DC-DC topology

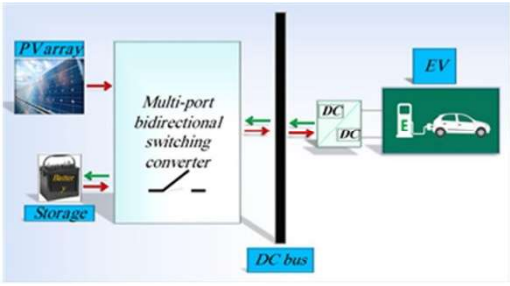

Fig. 1. Bidirectional multi-port DC-DC topology for electric vehicle

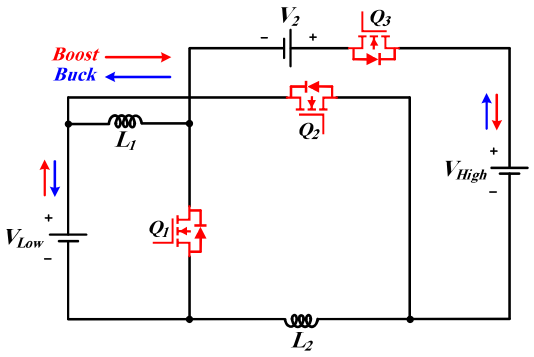

Fig. 2. The proposed converter

was suggested for PV supplied EVs. A multi-input multi-output transformer-less topology has been recommended in [18] for EVs applications. This converter can distribute power between input supplies and control of charge/discharge of the ES is properly obtained. In [19], a single inductor multi-input single-output converter with deadbeat-based control strategy has been suggested for EVs. In [15, 20], extendable multi-input single-output converter wee proposed for HESs. These topologies have higher voltage gain than that in similar works. However, they suffer from lack of bidirectional feature. In the current work, a bidirectional DC-DC structure with three ports is proposed for EV with HESs applications. The proposed converter can share a bidirectional power flow between the input and output ports. By selecting the appropriate duty cycles of the power switches, boost and buck operation modes are achieved. The suggested converter has a low voltage side, a high voltage side, and one auxiliary port. Also, it has only three power switches and two inductors, making it low in volume and cost. The basic benefit of this converter are low component count and high efficiency. In the rest of this paper, operation statues and steady-state analysis, design procedure, efficiency calculation, and comparison assessment are provided. Finally, to prove the theoretical survey, laboratory outcomes for boost and buck operations are presented.

2. OPERATION MODES AND STEADY-STATE ANALYSIS

The power circuit of the proposed topology is depicted in Fig. 2. As shown in this figure, three power MOSFETS (Q_1, Q_2, and Q_3) and two inductors (L_1 and L_2) are used. It has to be mentioned that L_1=L_2. The power switches have an internal anti-parallel diode. This topology can be worked in boost and buck operations. The current direction in boost and buck operation modes are shown by red and blue arrows, respectively. There are three ports: low voltage port (V_{Low}), high voltage port (V_{high}), and auxiliary port (V_2). Time waveforms of boost and buck operation are shown in Fig. 3. There are two switching states in each operation.

Nowadays, the tendency to achieve energy through the renewable sources has been increased sharply. One of the most common renewable sources is solar panels, which have many applications. The most important disadvantages of solar panels are their low output voltage and dependence on the environmental conditions. The multi-port converters are utilized in order to solve low output voltage problem, by combining the renewable sources. In multi-port converters the energy storage sources such as batteries can be used to solve the problem of dependence on their environmental conditions. The proposed converter is a multi-port bidirectional converter, which has the contribution of both multi-port converters and bidirectional converters. As seen in Fig. 1, V_{high} and V_{Low} are the bidirectional port of the suggested converter. V_2 is second source of the converter, which has been utilized for further increasing and decreasing the voltage conversion ratio in step-up and step-down modes, respectively. In step-up mode, the higher energy transferred to load via V_{low} and V_2 and subsequently, in step-down mode the lower energy is provided by using V_{high} and V_2. In fact in each operation modes, two ports acts as input sources and the other ports is the load.

A. Boost Operation

In this mode, the duty cycles of Q_1 and Q_2 (D_1) are higher than the duty cycle of Q_3 (D_2). By this switching pattern, the power is transferred from V_{low} to V_{high}, and boost operation is obtained.

State 1: In the first switching time, power switches Q_1 and Q_2 are turned on, and power switch Q_3 is turned off. Thus, inductors L_1 and L_2 start to charge by V_{low}, and their currents are increased during this time interval. Due to the boost operation, V_{high} is considered as the output port. The output load is supplied by the output capacitor (C_{high}). The configuration of status 1 has been depicted in Fig. 4(a). The following relations are obtained in this switching statues:

$$V_{L_1} = V_{L_2} = V_{Low} \quad (1)$$

$$V_{High} = V_{C_{High}} \quad (2)$$

$$i_{Low} = i_{L_1} + i_{L_2} = i_{Q_1} + i_{Q_2} \quad (3)$$

$$i_{C_{High}} = -I_{High} \quad (4)$$

State 2: At the start of status 2, the MOSFET Q_3 is switched on, and the MOSFETs Q_1 and Q_2 are switched off. The voltages across inductors L_1 and L_2 are negative, and their currents are decreased. In other words, the stored energy in these inductors along with the energy of V_2 are transferred to the high voltage port. The configuration of switching state 2 has been indicated in Fig. 4(b), and the relations of this statues are equal to:

$$V_{L_1} = V_{L_2} = \frac{V_{Low} + V_2 - V_{High}}{2} \quad (5)$$

$$i_{Low} = i_{L_1} = i_{L_2} = i_{Q_3} = i_{C_{High}} + I_{High} \quad (6)$$

Using equations Eq. (1) and Eq. (5), and applying volt-second balance low on L_1 and L_2, the relation between V_{high}, V_{low}, and V_2 can be calculated:

$$\langle V_{L_1} \rangle_{Ts} = \langle V_{L_2} \rangle_{Ts} = D_1 V_{Low} + (1 - D_1) \frac{V_{Low} + V_2 - V_{High}}{2} = 0 \quad (7)$$

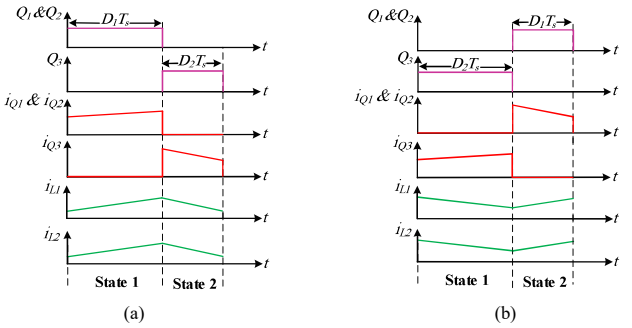

Fig. 3. Time waveforms, ***(a)*** Boost operation, ***(b)*** Buck operation.

$$V_{High} = V_2 + \frac{1+D_1}{1-D_1} V_{Low} = V_2 + \frac{1+D_1}{D_2} V_{Low} \quad (8)$$

Fig. 6(a) depicts the variation of V_{high} (V_h) versus D_1 and V_2 for V_{low}=20 V. It is apparent that by increasing the V_2, high voltage conversion ratio can be achieved.

B. Buck Operation

In buck mode, the duty cycle of Q_3 (D_2) is higher than the duty cycle of Q_1 and Q_2 (D_1). By this switching pattern, the power is transferred from V_{high} to V_{low}, and buck operation is obtained.

Status 1: In this switching time of the buck status, the Q_3 is switched on, and the MOSFETs Q_1 and Q_2 are switched off. Thus, the energy of V_{high}, L_1, and L_2 are transferred to V_{low} and V_2. The configuration of switching state 1 is depicted in Fig. 5(a), and the equation of this state are as follows:

$$V_{L_1} = V_{L_2} = \frac{V_{Low} + V_2 - V_{High}}{2} \quad (9)$$

$$i_{Q_3} = i_{High} = i_{L_1} = i_{L_2} = I_{Low} + i_{C_{Low}} \quad (10)$$

Status 2: In this switching state, power switches Q_1 and Q_2 are conducting, and the MOSFET Q_3 is switched off. Therefore, the voltage of V_{high} and V_2 remain constant, and C_{low} supplies the output load. The configuration of this switching state is demonstrated in Fig. 5(b), and the related relationships for this mode have been obtained as follows:

$$V_{L_1} = V_{L_2} = V_{Low} \quad (11)$$

$$i_{L_2} = i_{Q_2} \quad (12)$$

$$i_{L_1} = i_{Q_1} \quad (13)$$

$$I_{Low} = i_{Q_1} + i_{Q_2} + i_{C_{Low}} \quad (14)$$

Considering Eq. (9) and Eq. (11), and using volt-second balance low on L_1 and L_2, the relation between V_{low}, V_{high}, and V_2 in buck mode can be calculated:

$$\langle V_{L_1} \rangle_{Ts} = \langle V_{L_2} \rangle_{Ts} = D_2 \frac{V_{Low} + V_2 - V_{High}}{2} + (1 - D_2) V_{Low} = 0 \quad (15)$$

$$V_{Low} = \frac{D_2}{2D_1 + D_2} \left(V_{High} - V_2 \right) \quad (16)$$

Fig. 6(b) shows the variation of V_{low} versus D_1 and V_2 for V_{high}=90 V. As boost mode, the second DC supply (V_2) is utilized for further increasing the voltage gain.

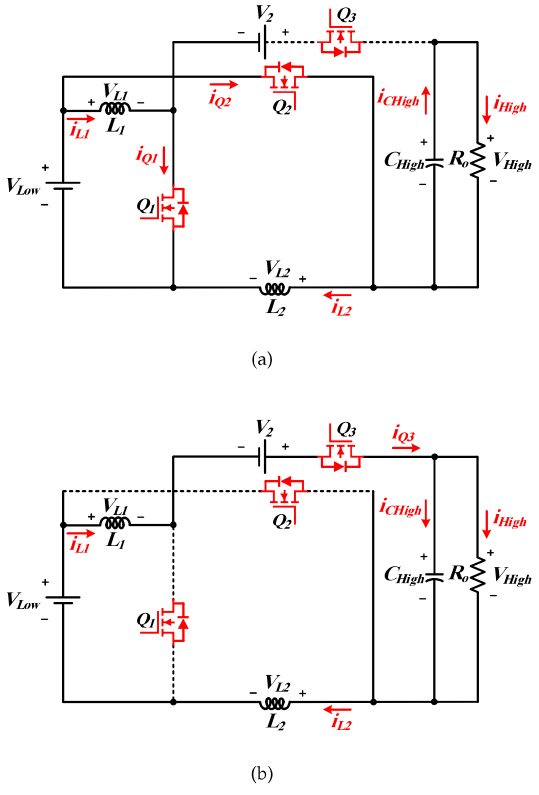

Fig. 4. The configuration of boost switching state, ***(a)*** state 1 of boost operation, ***(b)*** state 2 of boost operation.

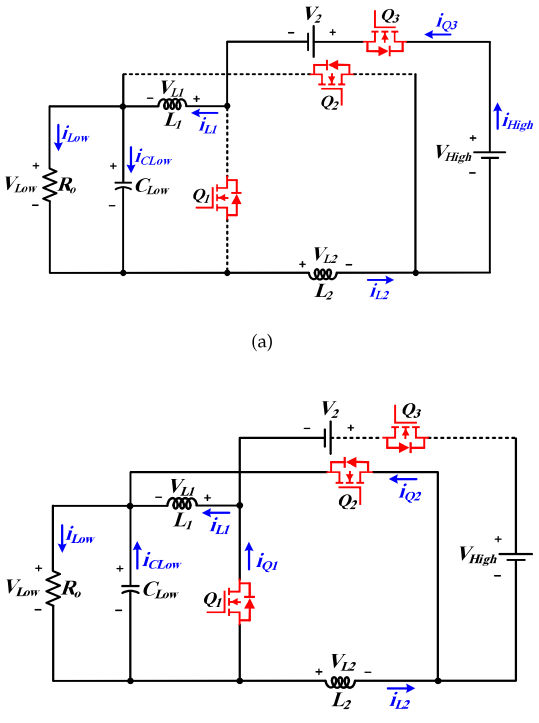

Fig. 5. The configuration of buck switching state, ***(a)*** state 1 of buck status, ***(b)*** state 2 of buck status.

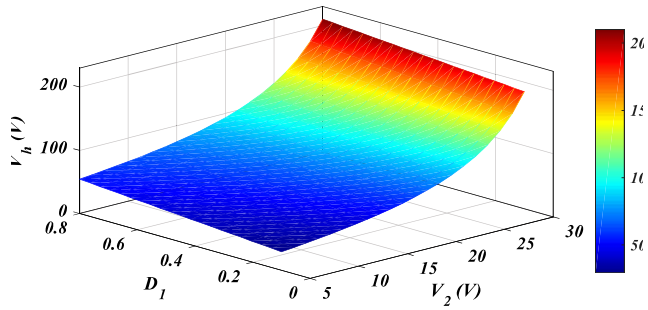

(a)

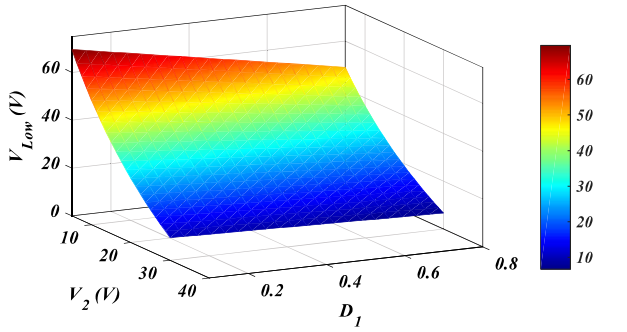

(b)

Fig. 6. Variation of V_{High} (V_h) and V_{Low} versus D_1 and V_2, ***(a)*** V_{High} , and ***(b)*** V_{Low}.

As seen in Fig. 1, V_{high} and V_{Low} are the bidirectional port of the suggested converter. V_2 is the second source of the converter, which has been utilized for further increasing and decreasing the voltage conversion ratio in step-up and step-down modes, respectively. In step-up mode, the higher energy transferred to load via V_{low} and V_2 and subsequently, in step-down mode the lower energy is provided by using V_{high} and V_2. In fact in each operation modes, two ports acts as input sources and the other ports is the load. From figure 4 of the main manuscript file, in step-up mode, in the first state the switches Q_1 and Q_2 are turned on and in the second state the switch Q_3 is turned on. Besides, from figure 5, in step-down mode, in first state the switch Q_3 is turned on and in the second mode the switches Q_1 and Q_2 are turned on. Also, by defining a reference current and voltage for the expected power level of the proposed converter, the current of the inductor and output voltage are read. If there is a change in the values of the input ports, the command to regulate the voltage at the output and the inductor current is applied through the microcontroller and it produces a suitable pulse for the power switches based on the load requirement. So based on the load requirement the following strategy can be defined for the recommended structure:

a) Two source are uses: In this case, both energy sources transfer to the load and increase the voltage gain of the proposed structure. In this functional mode, the storage system is charged in one operation mode and discharged in another operation mode. This functional mode can be used in electric vehicle applications to charge and discharge the battery. In this case, the second source is used to increase the conversion ratio of the output voltage in both charging and charging mode.

b) One source is used and other is off: This mode of operation occurs when the energy of the second source is zero. In this case, the first source, which is the main source of the proposed structure, performs the task of transferring power to the load lonely. This mode can be used in where the low power is needed.

3. STEADY-STATE ANALYSIS

A. Power Switches

The power switches are selected regarding the rated voltage and current. So, the voltage and current of these components are computed in each operation mode.

A.1. Boost Mode

Considering Fig. 4(b), the maximum voltage throughout the power MOSFETs Q_1 and Q_2 are expressed as follows:

$$V_{Q_1} = V_{High} - V_2 = \frac{1+D_1}{D_2} V_{Low} \tag{17}$$

$$\begin{aligned} V_{Q_2} &= \frac{1}{2}\left(V_{Low} + V_{High} - V_2\right) \\ &= \frac{1}{2}\left(V_{Low} + \frac{1+D_1}{D_2} V_{Low}\right) \\ &= \frac{1+D_1+D_2}{2D_2} V_{Low} \end{aligned} \tag{18}$$

The maximum voltage of MOSFET Q_3 is obtained in switching state 1, when this switch is turned off:

$$V_{Q_3} = V_{High} + V_{Low} - V_2 = \frac{1+D_1+D_2}{D_2} V_{Low} \tag{19}$$

Based on the proposed topology configuration, the average current of the low voltage port is achieved as Eq. (20):

$$I_{Low} = \frac{1+D_1}{D_2} I_{High} \tag{20}$$

The average current of Q_1 and Q_2 can be written versus inductors average current and I_{Low}:

$$I_{Q_1} = I_{L_1} - I_{Low} \tag{21}$$

$$I_{Q_2} = I_{L_2} - I_{Low} \tag{22}$$

On the other hand, the average current of the inductors L_1 and L_2 are explained as Eq. (23) and Eq. (24):

$$I_{L_1} = I_{Low} - I_{Q_2} = \frac{1+D_1}{D_2} I_{High} - I_{Q_2} \tag{23}$$

$$I_{L_2} = I_{Low} - I_{Q_1} = \frac{1+D_1}{D_2} I_{High} - I_{Q_1} \tag{24}$$

By calculating Eq. (21) - Eq. (24), the average currents of Q_1, Q_2, L_1, and L_2 are obtained as follows:

$$I_{L_1} = I_{L_2} = \frac{1+D_1+D_2}{D_2} I_{High} \tag{25}$$

$$I_{Q_1} = I_{Q_2} = \frac{1+D_1-D_2}{2D_2} I_{High} \tag{26}$$

Also, the average current of Q_3 is same as the average current of the high port voltage:

$$I_{Q_3} = I_{High} \tag{27}$$

Using the calculated average currents, the current stresses of the power switches are found as Eq. (28) and Eq. (29):

$$i_{Q_1} = i_{Q_2} = \frac{1+D_1-D_2}{2D_1D_2} I_{High} \tag{28}$$

$$i_{Q_3} = \frac{I_{High}}{D_2} \tag{29}$$

Finally, the root mean square (RMS) currents of the three MOSFETs in boost mode are computed as:

$$I_{Q_1}^{RMS} = I_{Q_2}^{RMS} = \frac{1 + D_1 - D_2}{2D_2\sqrt{D_1}} I_{High} \tag{30}$$

$$I_{Q_3}^{RMS} = \frac{I_{High}}{\sqrt{D_2}} \tag{31}$$

A.2. Buck Mode

Considering Fig. 4(a), the voltage stress throughout the MOSFETs Q_1 and Q_2 in buck mode are found as:

$$V_{Q_1} = V_{Q_2} = V_{Low} + \frac{V_{High} - V_{Low} - V_2}{2} = \frac{V_{Low}}{D_2} = \frac{V_{Low}}{1 - D_1} \tag{32}$$

Also, the voltage stress across Q_3 is calculated in switching state 2:

$$V_{Q_3} = V_{High} + V_{Low} - V_2 = \frac{2}{2D_1 + D_2}\left(V_{High} - V_2\right) \tag{33}$$

The average current in buck mode are obtained as Eq. (34) - Eq. (36):

$$I_{L_1} = I_{L_2} = I_{Low} \tag{34}$$

$$I_{Q_1} = I_{Q_2} = I_{Low} - I_{High} \tag{35}$$

$$I_{Q_3} = I_{High} \tag{36}$$

The peak current of the power MOSFETs can be defined follows:

$$i_{Q_1} = i_{Q_2} = \frac{2}{D_2}\left(I_{Low} - I_{High}\right) \tag{37}$$

$$i_{Q_3} = \frac{2I_{High}}{D_1} \tag{38}$$

It should be noticed that, the rated currents and voltages of the used switches in the experimental prototype are higher than the calculated values. The RMS currents of the power switches in buck mode are obtained as Eq. (39)-Eq. (40):

$$I_{Q_1}^{RMS} = I_{Q_2}^{RMS} = \frac{2}{\sqrt{D_2}}\left(I_{Low} - I_{High}\right) \tag{39}$$

$$I_{Q_3}^{RMS} = \frac{2I_{High}}{\sqrt{D_1}} \tag{40}$$

B. Inductors

Inductors L_1 and L_2 are designed to reach continuous current mode (CCM) operation. For this work, the current ripple is considered lower than half of the average current. The minimum value of each inductor is calculated by Eq. (41):

$$L \geq \frac{DV_L}{20\% f_s I_L} \tag{41}$$

The minimum content of inductors L_1 and L_2 in boost and buck operation modes are obtained as Eq. (42) and Eq. (43), respectively.

$$\begin{aligned} L_1 = L_2 \geq & \frac{2D_1D_2V_{Low}}{0.2f_s\left(1 + D_1 + D_2\right)I_{High}} \\ = & \frac{2D_1D_2^2\left(V_{High} - V_2\right)}{0.2f_s\left(1 + D_1\right)\left(\left(1 + D_1 + D_2\right)\right)I_{High}} \end{aligned} \tag{42}$$

$$\begin{aligned} L_1 = L_2 \geq & \frac{D_2V_{Low}}{0.2f_sI_{Low}} \\ = & \frac{2D_1D_2^2\left(V_{High} - V_2\right)}{0.2f_s\left(1 + D_1\right)\left(\left(1 + D_1 + D_2\right)\right)I_{High}} \end{aligned} \tag{43}$$

C. Capacitors

In each operation mode, only one capacitor is used as the output filter. The ripple is assumed lower than two percent of the output voltage to obtain a low output voltage ripple.

In boost mode, the minimum value of C_{High} is achieved as Eq. (44):

$$C_{High} \geq \frac{D_2 i_{C_{High}}}{0.02 f_s V_{C_{High}}} = \frac{D_2\left(I_{Low} - I_{High}\right)}{0.02 f_s V_{High}} \tag{44}$$

Also, the RMS current of this capacitor is found as Eq. (45):

$$I_{C_{High}}^{RMS} = \sqrt{I_{High}\left(D_1I_{High} + 2D_2I_{Low} + D_2I_{High}\right) + D_2I_{Low}^2} \tag{45}$$

In buck mode, the minimum value of C_{Low} and its RMS current are calculated as Eq. (46) and Eq. (47), respectively:

$$C_{low} \geq \frac{D_2 i_{C_{Low}}}{2\% f_s V_{Low}} = \frac{D_2\left(I_{High} - I_{Low}\right)}{2\% f_s V_{Low}} \tag{46}$$

$$I_{C_{Low}}^{RMS} = \sqrt{I_{High}^2\left(4D_1 + 2D_2\right) + I_{Low}^2 - 2I_{high}I_{Low}\left(2D_1 + D_2\right)} \tag{47}$$

4. EFFICIENCY CALCULATION

Section 4 presents the efficiency and power losses analysis of the recommended topology in both boost and buck operation modes.

A. Boost Mode

The total losses of the boost mode can be written as Eq. (48):

$$P_{Loss} = P_Q^{conduction} + P_Q^{switching} + P_{Magnetic} + P_C \tag{48}$$

The power switches losses include conduction and switching losses which are calculated as Eq. (49) and Eq. (55), respectively.

$$\begin{aligned} P_Q^{conduction} = & \frac{2}{D_1}\left(\frac{1 + D_1 - D_2}{2D_2}\right)^2 R_{DS-ON_{Q1,2}} {I_{High}}^2 \\ & + \frac{1}{D_2} R_{DS-ON_{Q3}} {I_{High}}^2 \end{aligned} \tag{49}$$

The inductors and capacitor total losses are found as follows:

$$P_{Magnetic} = \left(R_{L_1} + R_{L_2}\right)\left(\frac{1 + D_1 + D_2}{D_2} I_{High}\right)^2 \tag{50}$$

$$P_C = R_{C_{High}}\left(I_{High}\left(D_1I_{High} + 2D_2I_{Low} + D_2I_{High}\right) + D_2I_{Low}^2\right)^2 \tag{51}$$

Table 1. Summary of the Comparison results

Characteristics	[1]	[2]	[3]	[4]	[5]	[6]	[7]	[8]	Suggested
No. of Switches	4	4	4	4	2	2	3	6	3
No. of Diodes	5	4	3	1	3	2	5	2	-
No. of Inductors	2	2	1	1	2	2	2	4	2
No. of Capacitors	2	2	2	4	4	2	3	4	1
Used No. of Components	13	12	10	10	11	8	13	16	6
No. of Ports	4	4	4	4	3	3	4	3	3
Boost mode voltage rate	$\frac{1-D_1}{(1-D_2)(D_2-D_1)}$	$\frac{D^2-D+1}{(1-D)^2}$	$\frac{1}{1-D}$	$\frac{1}{1-D}$	3	$\frac{1-D_1+D_2}{1-D_1}$	$\frac{3}{1-D}$	$\frac{3-D}{1-2D+D^2}$	$\frac{2}{1-D}$
Peak voltage of semiconductors	V_{High}	$V_{High}-V_{Low}$	V_{High}	V_{High}	V_{High}	V_{High}	$\frac{V_{High}}{2}$	$\frac{V_{High}}{1-D}$	$V_{High}+V_{Low}-V_2$
Efficiency (%) at 100 W	-	90	-	-	97	-	-	94.8	94.8
Bidirectional	Yes	Yes	Yes	Yes	No	No	No	No	Yes
Frequency (kHz)	30	30	10	40	15	100	100	40	50

B. Buck Mode

The power switches conduction and switching losses of buck mode are calculated as Eq. (52) and Eq. (56), respectively.

$$P_Q^{conduction} = \frac{8}{D_2} R_{DS-ON_{Q1,2}} \left(I_{Low} - I_{High}\right)^2 + \frac{4}{D_2} R_{DS-ON_{Q3}} I_{High}^2 \quad (52)$$

Also, in buck operation, the losses of the inductors and the capacitor are found as follows:

$$P_{Magnetic} = \left(R_{L_1} + R_{L_2}\right) {I_{Low}}^2 \quad (53)$$

$$P_C = R_{C_{Low}} \left(I_{High}^2 \left(4D_1 + 2D_2\right) + I_{Low}^2 - 2I_{high} I_{Low} \left(2D_1 + D_2\right) \right)^2 \quad (54)$$

$$P_Q^{switching} = \frac{1}{2} f_s (t_{r_{Q1}} + t_{f_{Q1}}) \left(\frac{1+D_1}{D_2}\right) \left(\frac{1+D_1-D_2}{2D_2}\right) V_{Low} I_{High} + \frac{1}{2} f_s (t_{r_{Q2}} + t_{f_{Q2}}) \left(\frac{1+D_1+D_2}{2D_2}\right) \left(\frac{1+D_1-D_2}{2D_2}\right) V_{Low} I_{High} + \frac{1}{2} f_s (t_{r_{Q3}} + t_{f_{Q3}}) \frac{2}{2D_1+D_2} \left(V_{High} - V_2\right) \left(\frac{1+D_1-D_2}{2D_2}\right) I_{High} \quad (55)$$

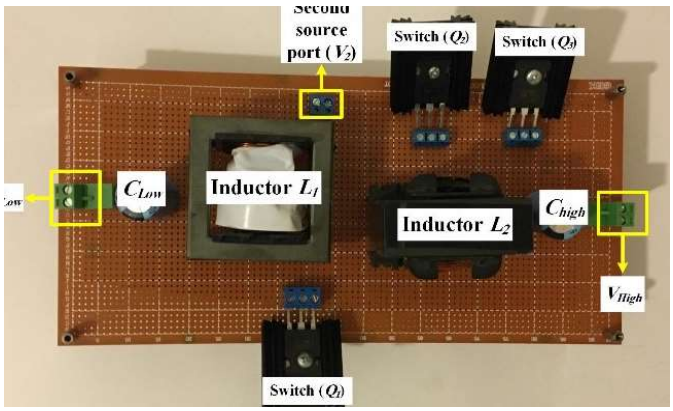

Fig. 7. Experimental prototype of the suggested converter.

$$P_Q^{switching} = f_s (t_{r_{Q1,2}} + t_{f_{Q1,2}}) \left(\frac{1}{1-D_1}\right) \left(I_{Low} - I_{High}\right) V_{Low} + \frac{1}{2} f_s (t_{r_{Q3}} + t_{f_{Q3}}) \frac{2}{2D_1+D_2} \left(V_{High} - V_2\right) I_{High} \quad (56)$$

5. COMPARISON ASSESSMENT

This sector proposes the comparison survey of the suggested bidirectional multi-port DC-DC topology and other same topologies (Refs [1], [2], [3], [4], [5], [6], [7], and [18]). In the current survey, the ports contents, MOSFET contents, diodes, inductors, capacitors, and total used components, the voltage gain in boost operation, maximum voltage across semiconductors, efficiency

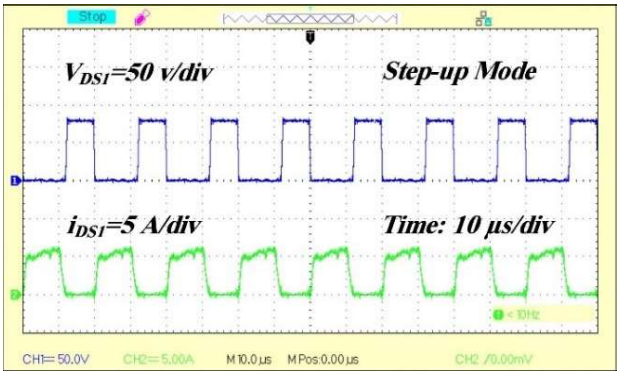

(a)

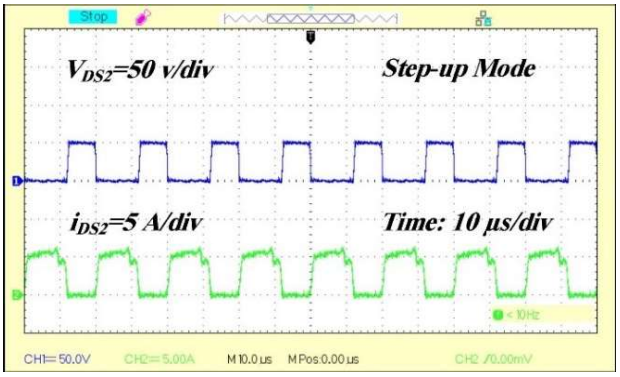

(b)

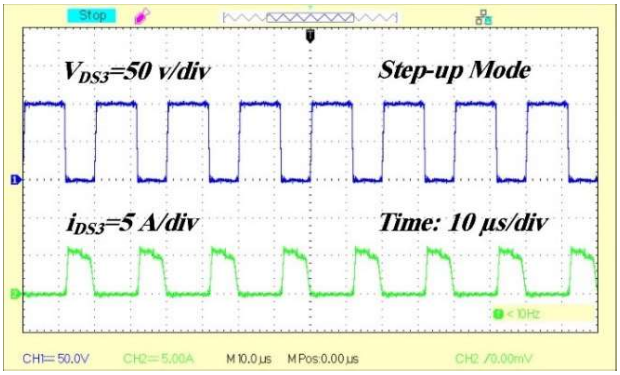

(c)

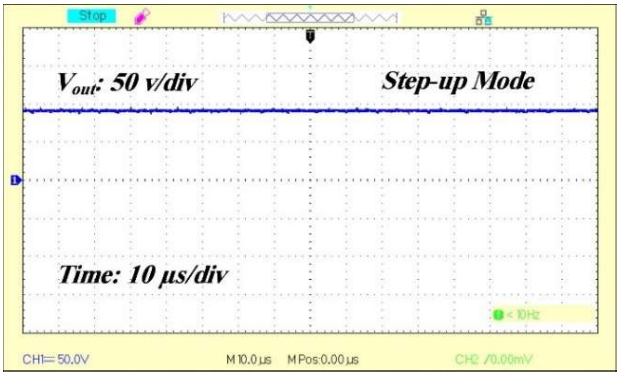

(d)

Fig. 8. The laboratory waveforms in step-up state, ***(a)*** $V_{Date-source\ 1} - i_{Drain\ --\ source\ 1}$, ***(b)*** $V_{Date-source\ 2} - i_{Drain\ --\ source\ 2}$, ***(b)*** $V_{Date-source\ 3} - i_{Drain\ --\ source\ 3}$, and ***(d)*** Output voltage.

Table 2. Component characteristics

Parameter	Boost Status	Buck Status
Input-voltage 1 (V_{in1})	20 V	90 V
Input-voltage 1 (V_{in2})	12 V	12 V
Rated power (P_{out})	170 W	90 W
Frequency (f_s)	50 kHz	50 kHz
Duty-cycle (D_1)	0.6	0.4
Duty-cycle (D_2)	0.4	0.6
Selected elements		
Capacitor C_L	200 V/220 µF	
Capacitor C_H	200 V/220 µF	
Switches (Q_1, Q_2 & Q_3)	IRFP260N	
Inductors L_1 & L_2	Ferric core (300 µH)	

at 100 W output power, bidirectional feature, and switching frequency are taken into account. As seen in Table 1 the critical factors of bidirectional DC-DC converters are proposed in order to show the superiority of the suggested structure.

The results of this survey are summarized in Table 1. Associated to this table, the number of utilized components in [8] is higher than the other topologies. In this converter, 6 power switches, 2 diodes, 4 magnetic cores, and 4 capacitors are used. So, it has a high cost and volume structure. On the other hand, the presented topology has only 6 used components. Also, it has no power diode in its structure. Thus, the proposed converter is more suitable regarding of the cost and the mass against the other introduced works in Table 1. The other impact of the low content of ingredients is high efficiency. The presented topology has 97.3 % efficiency at 100 W output power, which is higher than the others. The converters in [1], [2], [3], [4], and [7] have 4 independent ports. However, all of these topologies were built with a high number of components than the proposed converter. Efficiency for converters in [1], [3], [4], and [7] were not reported, and the topology in [2] has lower efficiency. The converters in [6] and [7] have higher switching frequency. This benefit leads to using low volume capacitors and inductors. However, these two converters suffer from lack of bidirectional feature. Therefore, it can be concluded that the proposed converter has required features for EVs applications such as multi-port and bidirectional with low components count and high efficiency.

6. EXPERIMENTAL RESULTS

In this sector, the presented topology has been accomplished and tested in the laboratory. The components specifications and selected devices are demonstrated in Table 2. It has to be mentioned that the recommended topology is tested in both boost and buck status. The obtained results in this part proves the correctness of the theoretical survey and mathematical calculations.

The experimental prototype is added and is shown in Fig. 7.

A. Step-Up State

The basic laboratory waveforms of the proposed circuit in this mode are depicted in Figs. 8–9. The voltage and current waveforms of the MOSFETs are depicted in Figs. 4(a)–8(c). From

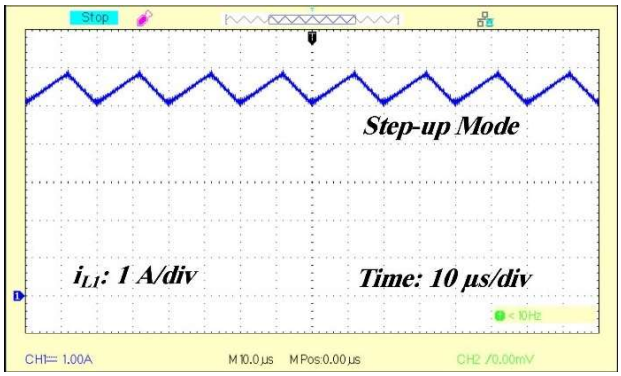

(a)

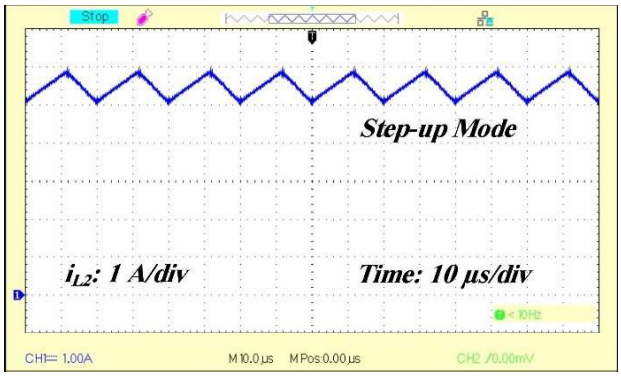

(b)

Fig. 9. The laboratory measurement in boost state, ***(a)*** i_{L1} and ***(b)*** i_{L2}.

Fig. 8, it can be found that in the first status of boost operation the MOSFET Q_1 is switched on and by contrast, in the other mode of this state the MOSFETs Q_2 and Q_3 are switched on. The voltage and current of the switch Q_1 are about 80 V and 6 A, respectively, as is shown in Fig. 8(a). The voltage and current measurement of the switch Q_2 are illustrated in Fig. 8(b), which are almost 50 V and 6 A, respectively. The voltage and current of switch Q_3, indicated in Fig. 8(c), are approximately 100 V and 6 A, respectively. The output voltage waveform of the suggested converter in this operation mode is indicated in Fig. 8(d). Regarding this figure, the input voltage of 20 V and 12 V are increased to almost 92 V with poor voltage ripple. Thus, the suggested converter has appropriate voltage conversion ratio. The inductors L_1 and L_2 waveforms are displayed in Figs. 9(a) and 9(b), respectively. Related to this figure, that is apparent that the ripple throughout the inductors have small value in this operation state.

B. Step-Down State

The main laboratory measurements of the recommended structure in step-down mode have been demonstrated in Figs. 10–11. The voltage and current measurements of the MOSFETs are depicted in Figs. 10(a)–10(d). From Fig. 10, it is apparent that at the first operation state of step-down status the MOSFETs Q_2 and Q_3 are switched on and in other side, at the second state of this status the MOSFET Q_1 is switched on. The drain – source voltage and current waveforms of the switches Q_1 and Q_2 are equal each other and are 55 V and 2.4 A, respectively that are indicated in Fig. 10(a) and 10(b), respectively. The voltage and current measurement of switch Q_3 are illustrated in Fig. 10(c), which are

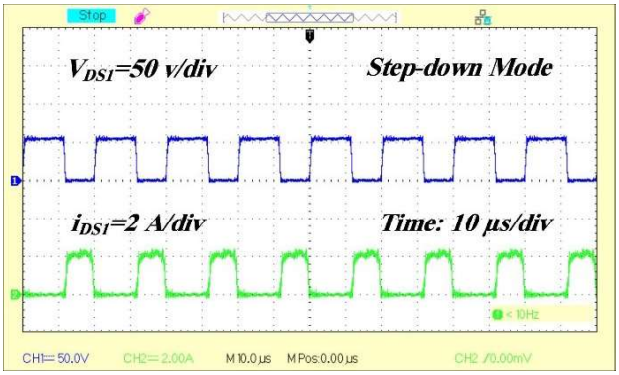

(a)

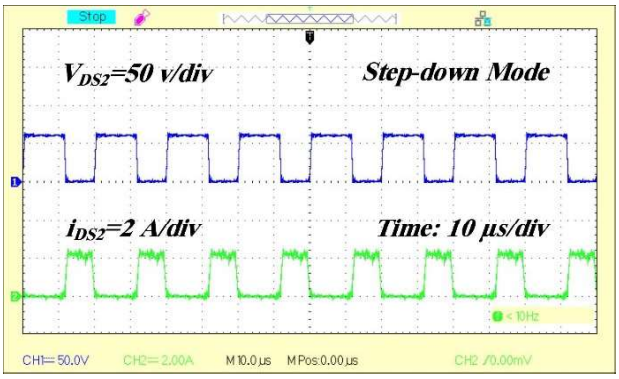

(b)

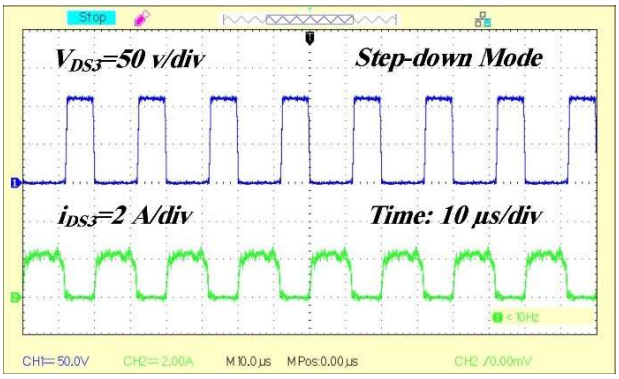

(c)

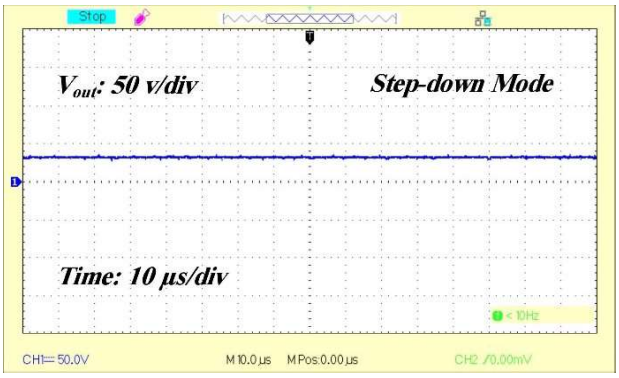

(d)

Fig. 10. The laboratory waveforms in step-down state, ***(a)*** $V_{Date-source\ 1} - i_{Drain\ --\ source\ 1}$, ***(b)*** $V_{Date-source\ 2} - i_{Drain\ --\ source\ 2}$, ***(b)*** $V_{Date-source\ 3} - i_{Drain\ --\ source\ 3}$.

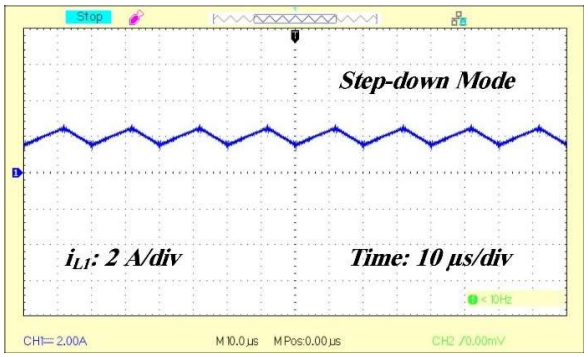

(a)

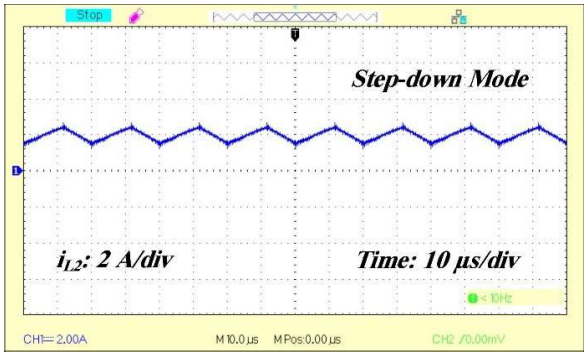

(b)

Fig. 11. The laboratory waveforms in step-down state, ***(a)*** i_{L1} and ***(b)*** i_{L2}.

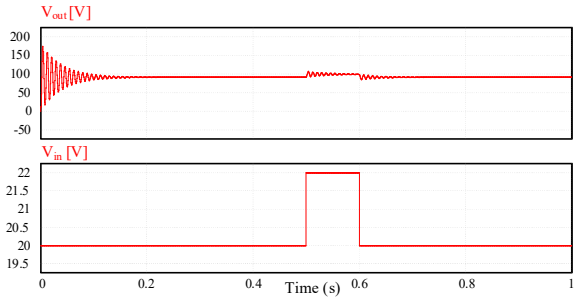

(a)

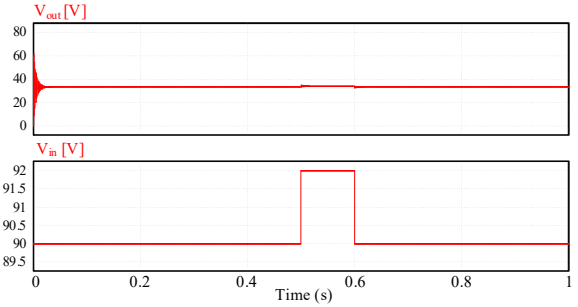

(b)

Fig. 12. Transient response of the proposed converter, (a) Step-up mode, (b) Step-down mode.

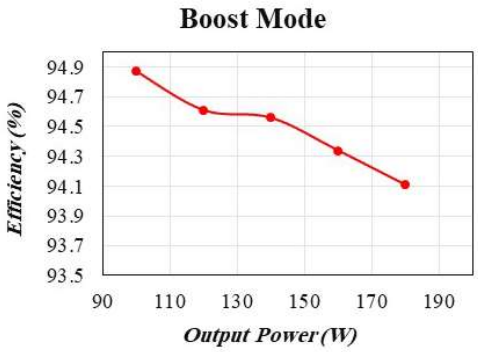

(a)

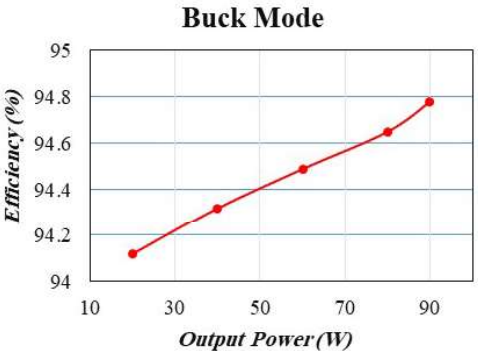

(b)

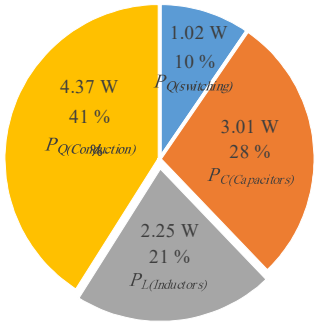

(c)

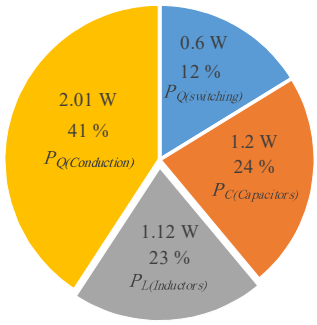

(d)

Fig. 13. Efficiency survey plot and losses plot based on obtained values for elements, ***(a)*** Efficiency plot varied load power in boost status, ***(b)*** Efficiency plot varied load power in buck status, ***(c)*** Loss plot in boost status, and ***(d)*** loss plot in buck status.

almost 110 V and 2.4 A, respectively. The load voltage measurement of the recommended structure in this operation state is demonstrated in Fig. 10(d). From this figure, the input voltages of 90 V and 12 V in step-down mode are decreased about 33 V with low voltage ripple. As in the boost mode, the suggested converter in buck mode has appropriate voltage gain. The inductors L_1 and L_2 waveforms are demonstrated in Figs. 11(a) and 11(b), respectively. Related this figure, it is apparent that the ripple value of the inductors in step-down mode is low.

Related to the theoretical analysis, comparison survey and the laboratory result, it is clear that the used semiconductor elements in the proposed topology have presented at a low peak voltage, which results in lower cost and higher efficiency of the converter. Besides, it has been shown that in the proposed structure, efficiency is flexible that show the suggested converter has ability to operate in high power rating in industry application. Therefore, by using high power rating elements in laboratory prototype, the proposed converter can be utilized in low power applications PV/ battery power generations in electric vehicles or hybrid electric vehicles.

The transient response of the proposed converter for step-change about 2V in input voltage is illustrated in Fig. 12. Based on thisfigure, it is clear that the proposed converter has a good dynamic response for the step-change in the input voltage for both step-up and step-down mode.

The proposed converter efficiency diagram based on output power in both boost and buck operating modes is shown in Fig. 13(a) and 13(b), respectively. The obtained efficiency for boost mode is calculated by considering the values of V_{low} = 20 V, V_2 = 12 V, V_{out} = 92 V, D_1 = 0.6, D_2 = 0.4. Moreover, the efficiency of the recommended converter is calculated for V_{high} = 90 V, V V_{low} = 12, V_{out} = 42 V, D_1 = 0.4, D_2 = 0.6 for the buck mode. Besides, the power loss diagram for the mentioned values in both boost mode (170 W) and buck mode (90 W) is demonstrated in Fig. 13(c) and 13(d), respectively. Depending on these figures, the efficiency of the recommended converter is varied from light load to full load. Therefore, the suggested structure can be a suitable selection for green energy usages and electric vehicles with combined power supplies.

7. CONCLUSIONS

This paper proposed a multi-port bidirectional DC-DC topology of DC-DC converter for EV with HESs applications. The suggested converter has a low voltage port, a high voltage port, and one auxiliary port. This topology has the ability to operate in boost and buck modes and share a bidirectional power flow between low voltage and high voltage ports. The main advantages of this converter are low components count, low volume, low cost, and high efficiency. In order to illustrate the effectiveness of the proposed converter, the working status and steady-state analysis, design procedure, efficiency calculation, and comparison assessment are provided. Finally, to verify the theoretical analysis, experimental results for boost operation in V_{low}=20, V_2=12 and buck operations in V_{high}=90, V_2=20 are presented, where the boost and buck modes efficiency are obtained 94.3 % in 90 V output voltage and 94.8% in 33 V output voltage, respectively. According to the recorded analysis and obtained results in each section, the suggested topology can be used in hybrid power systems such as PV/batteries or PV/fuel cells power generation and also can be used in hybrid electric vehicles with energy storage system.

REFERENCES

1. Ahrabi, R. R., Ardi, H., Elmi, M., Ajami, A.: A novel step-up multiinput DC–DC converter for hybrid electric vehicles application. IEEE Trans. Power Electron. 32, 3549-3561 (2016). https://doi.org/10.1109/TPEL.2016.2585044
2. Kardan, F., Alizadeh, R., Banaei, M. R.: A new three input DC/DC converter for hybrid PV/FC/battery applications. IEEE J. Emerging Sel. Top. Power Electron. 5, 1771-1778 (2017). https://doi.org/10.1109/JESTPE.2017.2731816
3. Nahavandi, A., Hagh, M. T., Sharifian, M. B. B., Danyali, S.: A nonisolated multiinput multioutput DC–DC boost converter for electric vehicle applications. IEEE Trans. Power Electron. 30, 1818-1835 (2014). https://doi.org/10.1109/TPEL.2014.2325830
4. Mohseni, P., Hosseini, S., Maalandish, M., Sabahi, M.: Ultra-high step-up two-input DC–DC converter with lower switching losses. IET Power Electron. 12, 2201-2213 (2019). https://doi.org/10.1049/iet-pel.2018.5924
5. Deihimi, A., Mahmoodieh, M. E. S., Iravani, R.: A new multi-input step-up DC–DC converter for hybrid energy systems. Electr. Power Syst. Res. 149, 111-124 (2017). https://doi.org/10.1016/j.epsr.2017.04.017
6. Zhou, L. W., Zhu, B. X., Luo, Q. M.: High step-up converter with capacity of multiple input. IET Power Electron. 5, 524-531 (2012). https://doi.org/10.1049/iet-pel.2011.0177
7. Yuan-mao, Y., Cheng, K. W. E.: Multi-input voltage-summation converter based on switched-capacitor. IET Power Electron. 6, 1909-1916 (2013). https://doi.org/10.1049/iet-pel.2013.0015
8. Pourjafar, S., Shayeghi, H., Sedaghati, F., Seyedshenava, S., Blaabjerg, F.: A bidirectional multiport DC-DC converter applied for energy storage system with hybrid energy sources. Int. J. Circuit Theory Appl. 49, 2453-2478 (2021). https://doi.org/10.1002/cta.2988
9. Shayeghi, H., Pourjafar, S., Hashemzadeh, S. M., Blaabjerg, F.: A high efficiency soft-switched DC–DC converter with high voltage conversion ratio. Int. J. Circuit Theory Appl. 49, 244-266 (2021). https://doi.org/10.1002/cta.2930
10. Pourjafar, S., Shayeghi, H., Hashemzadeh, S. M., Sedaghati, F., Maalandish, M.: A non-isolated high step-up DC–DC converter using magnetic coupling and voltage multiplier circuit. IET Power Electron. 14, 1637-1655 (2021). https://doi.org/10.1049/pel2.12139
11. Saadatizadeh, Z., Babaei, E., Blaabjerg, F., Cecati, C. Three-port high step-up and high step-down dc-dc converter with zero input current ripple. IEEE Trans. Power Electron. 36, 1804-1813 (2020). https://doi.org/10.1109/TPEL.2020.3007959
12. Pourjafar, S., Sedaghati, F., Shayeghi, H., Maalandish, M.: High step-up DC–DC converter with coupled inductor suitable for renewable applications. IET Power Electron. 12, 92-101 (2019). https://doi.org/10.1049/iet-pel.2018.5414
13. Ahrabi, R. R., Ardi, H., Elmi, M., Ajami, A.: A novel step-up multiinput DC–DC converter for hybrid electric vehicles application. IEEE Trans. Power Electron. 32, 3549-3561 (2016). https://doi.org/10.1109/TPEL.2016.2585044
14. Pourjafar, S., Shayeghi, H., Hashemzadeh, S. M., Sedaghati, F., Maalandish, M.: A non-isolated high step-up DC–DC converter using magnetic coupling and voltage multiplier circuit. IET Power Electron. 14, 1637-1655 (2021). https://doi.org/10.1049/pel2.12139
15. Pourjafar, S., Shayeghi, H., Sedaghat, F., & SeyedShenava, S.: A dual-input DC-DC structure with high voltage gain suggested for hybrid energy systems. IET Power Electron. 14, 1792-1805 (2021). https://doi.org/10.1049/pel2.12149
16. Akar, F., Tavlasoglu, Y., Ugur, E., Vural, B., Aksoy, I.: A bidirectional nonisolated multi-input DC–DC converter for hybrid energy storage systems in electric vehicles. IEEE Trans. Veh. Technol. 65, 7944-7955. (2015). https://doi.org/10.1109/TVT.2015.2500683
17. Guru Kumar, G., Sundaramoorthy, K., Athikkal, S., Karthikeyan, V.: Dual input superboost DC–DC converter for solar powered electric vehicle. IET Power Electron. 12, 2276-2284 (2019). https://doi.org/10.1049/iet-pel.2018.5255
18. Naderi, E., Seyedshenava, S. J., Shayeghi, H.: High Gain DC/DC Converter Implemented with MPPT Algorithm for DC Mi-

crogrid System. J. Oper. Autom. Power Eng. 11, 213-222 (2023). https://doi.org/10.22098/joape.2023.10270.1731
19. Wang, B., Zhang, X., Gooi, H. B.: An SI-MISO boost converter with deadbeat-based control for electric vehicle applications. IEEE Trans. Veh. Technol. 67, 9223-9232 (2018). https://doi.org/10.1109/TVT.2018.2853738
20. Banaei, M. R., Ajdar Faeghi Bonab, H., Taghizadegan Kalantari, N.: Analysis and design of a new single switch non-isolated buck-boost dc-dc converter. Journal of Operation and Automation in Power Engineering. 8, 116-127 (2020). https://doi.org/10.22098/joape.2019.5363.1403
21. Yuan-mao, Y., Cheng, K. W. E.: Multi-input voltage-summation converter based on switched-capacitor. IET Power Electron. 6, 1909-1916 (2013). https://doi.org/10.1049/iet-pel.2013.0015
22. Varesi, K., Hosseini, S. H., Sabahi, M., Babaei, E., Saeidabadi, S., Vosoughi, N.: Design and analysis of a developed multiport high step-up DC–DC converter with reduced device count and normalized peak inverse voltage on the switches/diodes. IEEE Trans. Power Electron. 34, 5464-5475 (2018). https://doi.org/10.1109/TPEL.2018.2866492